Journal of Medicinal Chemistry

Article

pubs.acs.org/jmc

Lead Optimization of a Pyrazole Sulfonamide Series of *Trypanosoma brucei N*-Myristoyltransferase Inhibitors: Identification and Evaluation of CNS Penetrant Compounds as Potential Treatments for Stage 2 Human African Trypanosomiasis

Stephen Brand, Neil R. Norcross, Stephen Thompson, Justin R. Harrison, Victoria C. Smith, David A. Robinson, Leah S. Torrie, Stuart P. McElroy, Irene Hallyburton, Suzanne Norval, Paul Scullion, Laste Stojanovski, Frederick R. C. Simeons, Daan van Aalten, Julie A. Frearson, Ruth Brenk, Alan H. Fairlamb, Michael A. J. Ferguson, Paul G. Wyatt, Ian H. Gilbert,* and Kevin D. Read*

Drug Discovery Unit, Division of Biological Chemistry and Drug Discovery, College of Life Sciences, University of Dundee, Sir James Black Centre, Dundee DD1 5EH, U.K.

Supporting Information

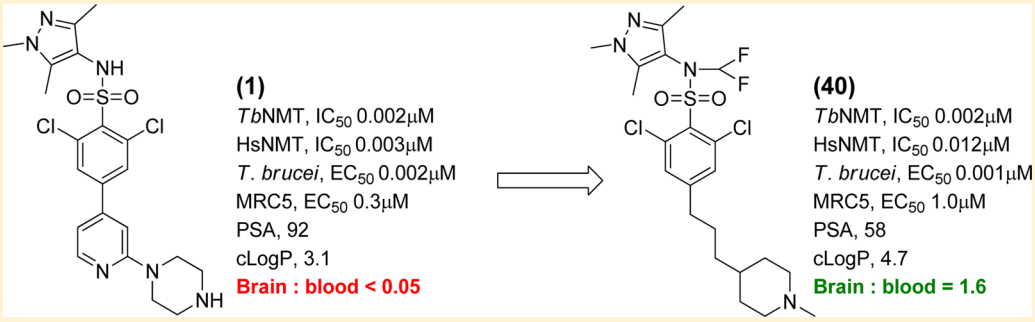

ABSTRACT: *Trypanosoma brucei N*-myristoyltransferase (*Tb*NMT) is an attractive therapeutic target for the treatment of human African trypanosomiasis (HAT). From previous studies, we identified pyrazole sulfonamide, DDD85646 (**1**), a potent inhibitor of *Tb*NMT. Although this compound represents an excellent lead, poor central nervous system (CNS) exposure restricts its use to the hemolymphatic form (stage 1) of the disease. With a clear clinical need for new drug treatments for HAT that address both the hemolymphatic and CNS stages of the disease, a chemistry campaign was initiated to address the shortfalls of this series. This paper describes modifications to the pyrazole sulfonamides which markedly improved blood−brain barrier permeability, achieved by reducing polar surface area and capping the sulfonamide. Moreover, replacing the core aromatic with a flexible linker significantly improved selectivity. This led to the discovery of DDD100097 (**40**) which demonstrated partial efficacy in a stage 2 (CNS) mouse model of HAT.

INTRODUCTION

Human African trypanosomiasis (HAT) is caused by two subspecies of the protozoan parasite *Trypanosoma brucei*, *Trypanosoma brucei gambiense* and *Trypanosoma brucei rhodesiense*, transmitted by the bite of an infected tetse fly.[1,2] The disease is fatal unless treated. It has two stages: an initial (hemolymphatic) peripheral infection during which the parasites are found in the bloodstream and gives rise to nonspecific symptoms, and a second stage during which the parasites enter the central nervous system (CNS), giving rise to the classic symptoms of HAT, eventually leading to coma and death. Currently, there are five treatments available, although none of them are satisfactory, due to toxicity, treatment failures, and the requirement for parenteral administration that is inappropriate in a rural African setting.[3]

N-Myristoyltransferase (NMT) catalyzes the cotranslational transfer of myristate from myristoyl-CoA to the *N*-terminal glycine of a large number of proteins, a modification which is implicated in localization and/or activation of the substrate.[4,5] The enzyme operates via a Bi−Bi mechanism in which it first binds myristoyl-CoA, causing a conformational rearrangement, which subsequently reveals the peptide binding site.[6] In *T. brucei*, RNAi knockdown of NMT has been shown to be lethal in cell culture[7] and to abrogate infectivity in animal models of HAT.[8] Bioinformatics analysis suggests that about 60 proteins are myristoylated in the parasite,[9] although there is incomplete knowledge of the downstream targets.[10] NMT has also been investigated as a potential target for the treatment of other parasitic diseases including malaria,[11] leishmaniasis,[12] and Chagas disease.[13]

Received: May 27, 2014
Published: November 20, 2014

   dx.doi.org/10.1021/jm500809c | *J. Med. Chem.* 2014, 57, 9855−9869

Recently, we have reported the discovery of DDD85646 (**1**, Figure 1), a very potent inhibitor of *T. brucei* NMT (*Tb*NMT)

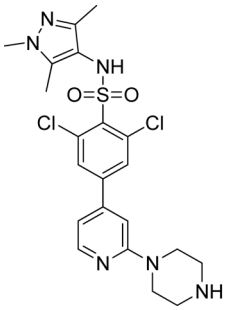

DDD85646 (1)
*Tb*NMT, IC_{50} 0.002μM
*Hs*NMT, IC_{50} 0.003μM
T. brucei, EC_{50} 0.002μM
MRC5, EC_{50} 0.3μM
Brain : blood < 0.05 (mouse)
Mw, 495.4
PSA, 92
cLogP, 3.1
Plasma protein binding, 94% (mouse)

Figure 1. Biological and physicochemical profile of the prototypical NMT inhibitor **1**.

(IC_{50} = 0.002 μM) and of the growth of *T. brucei* (EC_{50} = 0.002 μM), which delivers potent activity in mouse models of stage 1 HAT (fully curative at 12.5 mg/kg b.i.d. po for 4 days, *T. b. brucei* S427; fully curative at 50 mg/kg b.i.d. po for 4 days, *T. b. rhodesiense* STIB900).[14] Combined with further biological mode of action studies, this has provided excellent validation of NMT as a therapeutic target for the peripheral stage of HAT.[15]

Unfortunately, **1** is not active in the stage 2 HAT mouse model (*T. b. brucei* GVR35; 100 mg/kg b.i.d. po for 5 days).[14,15] However, this was unsurprising, as **1** poorly penetrates the blood–brain barrier and is a substrate for P-glycoprotein, thus preventing delivery of efficacious free brain concentration at a tolerated dose (blood:brain ratio is <0.05 in mouse and <0.09 in rat, rising to 0.27 in rat in the presence of the Pgp inhibitor GF120918;[16] experimental in Supporting Information). Furthermore, **1** has relatively poor/no selectivity at the enzyme level compared to the two human orthologues *Hs*NMT1 and *Hs*NMT2 (IC_{50} = 0.003 μM), although this did not translate to low selectivity at the cellular level (cellular selectivity ratio, MRC-5 EC_{50}/*T. brucei* EC_{50} = 150). While there was no observable toxicity in rodents at therapeutic doses, there was a relatively low therapeutic index (stage 1 HAT minimal curative dose = 12.5 mg/kg b.i.d. po [*T. b. brucei* S427] or 50 mg/kg b.i.d. po [*T. b. rhodesiense* STIB900]; MTD = 100 mg/kg b.i.d. po). It is unknown if the low safety margin in vivo is caused by inhibition of mouse NMT or another off-target effect. However, to try and eliminate the former, it was decided to improve the enzymatic selectivity. Typically, selectivity between two enzymes of interest is expressed as a ratio of their biochemical IC_{50} values (which in this case would be *Hs*NMT/*Tb*NMT). However, during the course of this study, we discovered that many compounds were very potent inhibitors of *Tb*NMT, which due to the enzyme concentration used in the assay (10 nM) have IC_{50} values approaching the observable tight-binding limit (as evidenced by Hill slopes ≫1) and there is thus very little differentiation between the most potent compounds. Because we have already shown for this series that *Tb*NMT IC_{50} is proportional to *T. brucei* EC_{50}, our preferred means of defining selectivity (*S*) was therefore to use activity against the parasite as a surrogate for *Tb*NMT IC_{50} when comparing activity against inhibition of *Hs*NMT, to give a good rank order:

$$S = IC_{50}HsNMT/EC_{50}T.\ brucei$$

RESULTS AND DISCUSSION

In this paper, we report the systematic optimization of both the blood–brain barrier penetration and selectivity of **1**, which has led to the discovery of CNS penetrant *Tb*NMT inhibitors suitable for progression into in vivo proof-of-concept studies in mice for the second stage of HAT. A summary of our structure–activity findings is shown in Figure 2.

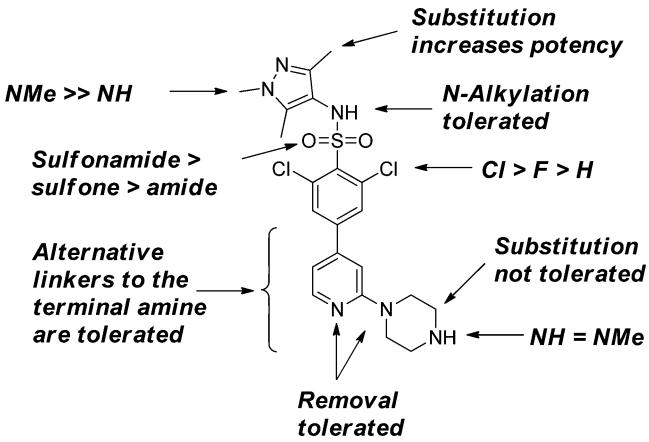

Figure 2. Summary of structure–activity relationships of (**1**).

Unfortunately, we were unable to obtain crystal structures of *Tb*NMT. However, we were able to obtain structural information for the *Leishmania major* NMT (*Lm*NMT) and *Aspergillus fumigatus* NMT (*Af*NMT). The *Tb*NMT, *Lm*NMT, *Af*NMT, and *Hs*NMT have very high sequence identity in the binding site for these class of inhibitors (Supporting Information, Table S7). Therefore, we decided to use the *Lm*NMT and *Af*NMT as surrogates. These should be of use in determining the binding mode of the inhibitors and suggesting vectors for chemistry optimization. However, given the similarities of the active sites, using the crystallography to derive selectivity may be very challenging, especially where factors such as the conformational flexibility of the protein and interactions with water may play a key role.

Optimization of the Pyrazole Head Group. We had previously shown that we were unable to vary the pyrazole headgroup for other heterocycles without significant loss in potency and that removal of the *N*-methyl or replacements with other alkyl groups gave a significant loss in activity.[14] From the *Leishmania major* cocrystal structure with **1**, the N1-methyl group binds in a hydrophobic pocket and is important in fixing N2 as hydrogen bond acceptor in a key hydrogen bonding interaction with the hydroxyl side chain of a highly conserved serine residue. However, substituents bigger than methyl on N1 would be expected to suffer a clash in the active site (see Figure 3).

The importance of both the pyrazole 3- and 5-methyl groups can be seen by comparing **2**, **3**, and **4** with **1** (see Table 1), which were prepared according to Scheme 1. It was possible to remove each of the methyls independently without affecting the enzyme potency, but removal of both methyls caused a significant loss in enzyme potency. Interestingly, removal of the 3-methyl group appeared to cause a reduction in parasite potency in contrast to removal of the 5-methyl group (i.e., **2** vs **3**). The 3- and 5-methyl groups both make hydrophobic contacts with the protein. It was possible to increase the size of the substituent at either the 3- or 5-positions (**5** and **6**),

dx.doi.org/10.1021/jm500809c | J. Med. Chem. 2014, 57, 9855–9869

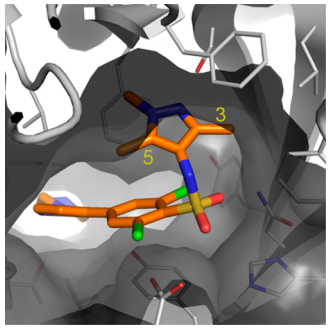

Figure 3. Crystal structure of **1** bound to *Lm*NMT (PDB 2WSA), highlighting the pyrazole sulfonamide pocket. The pyrazole *N*-methyl packs tightly into the hydrophobic pocket, however, there is scope to project from the 3- and 5- substituents and the solvent exposed sulfonamide nitrogen.

although there was no apparent increase in enzyme potency. However, the *iso*-butyl substituent on the 3-position (**6**) gave a significant increase in activity against the parasite.

As well as being one of the most active compounds from this series, compound **6** also benefited from having nearly a 10-fold higher oral exposure in mouse than **1** (10 mg/kg po AUC_{0-8}, 3400 μg min/mL cf. 392 μg min/mL; bioavailability 93% cf. 20 %) and correspondingly demonstrated superior efficacy to **1** in the stage 1 model in mice infected with *T. b. rhodesiense* STIB900 (minimal curative dose was 6 mg/kg cf. 50 mg/kg when dosed for 4 days b.i.d. po). Although it had higher efficacy

Scheme 1. Synthesis of Compounds in Table 1[a]

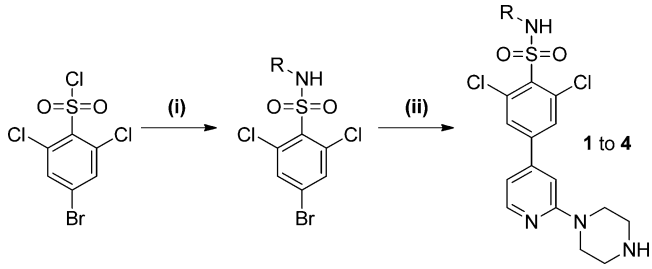

[a](i) RNH_2, pyridine/DCM; (ii) $Pd(PPh_3)_4$, 2-(1-piperazinyl)pyridine-4-boronic acid pinacol ester, K_3PO_4, THF/H_2O.

than **1**, compound **6** was nonselective, with no overall improvement in stage 1 HAT therapeutic window (2−3-fold; MTD in mice 20 mg/kg b.i.d. po). Indeed, the very high potency of **6** for *Hs*NMT could be the driving force for a high antiproliferative effect against the MRC-5 cell line (EC_{50} = 0.090 μM), thus eliminating it from further progression for HAT. Moreover, compound **6** also had very low brain penetration in mouse (brain:blood ratio <0.1). So, although potency was increased, there was no overall gain in terms of selectivity or brain penetration.

Investigation of SAR at the Central Aromatic Ring. One or both of the chloro substituents on the central aromatic ring of **1** were replaced with fluorine, methyl, or hydrogen, intended to modulate localized van der Waals interactions, but this did not have a significant effect on activity or selectivity for

Table 1. Modifications to the Head Group Pyrazole

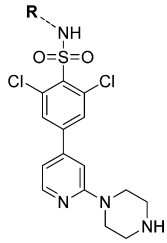

No.	R	*Tb*NMT IC_{50} (μM)[a]	*Hs*NMT IC_{50} (μM)[a]	*T. brucei* EC_{50} (μM)	S	B:B	MRC-5 EC_{50} (μM)
1		0.002[b]	0.003	0.002	1.5	< 0.1	0.30
2		0.005	0.009	0.024	< 1	nd	1.23
3		0.004[b]	0.012	0.002	6.0	nd	0.25
4		0.039	0.059	0.37	< 1	nd	10.3
5		0.006	0.025	0.005	5.0	nd	0.64
6	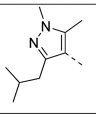	0.002[b]	0.004	0.0004	10	< 0.1	0.09

[a]IC_{50} values are shown as mean values of two or more determinations. Standard deviation is typically within 2-fold from the IC_{50}. [b]Compounds with Hill slopes >1.5. *S* = IC_{50} *Hs*NMT/EC_{50}*T. brucei*. B:B is the brain:blood ratio in mouse. nd = not determined.

dx.doi.org/10.1021/jm500809c | *J. Med. Chem.* 2014, 57, 9855−9869

*Tb*NMT (see Scheme S1 and Table S1, Supporting Information).

Optimization of the Piperazine Ring. It was decided to investigate the influence of substituents α- to the terminal nitrogen of the piperazine on the selectivity of **1**. Reference to the structure of **1** in *Lm*NMT showed a pocket which was not accessed but could accommodate extra functionality (see Figure S1, Supporting Information). This investigation found that small substituents were tolerated but did not give a significant rise in selectivity, *S*. Larger substituents caused a loss in activity (see Scheme S2 and Table S2, Supporting Information).

The effect of removing one or both of the pyridyl and internal piperazine nitrogens (Scheme 2) was investigated with

Scheme 2. Synthesis of Compounds in Table 2[a]

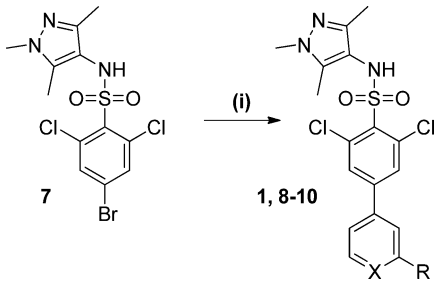

[a](i) $Pd(PPh_3)_4$, K_3PO_4, THF/H_2O and a boronate ester, (2-(1-piperazinyl)pyridine-4-boronic acid pinacol ester for compound **1**, 2-(1-piperazinyl)phenyl-4-boronic acid pinacol ester for compound **8**, 2-(4-piperidinyl)phenyl-4-boronic acid pinacol ester for compound **9**, and 2-(4-methyl-1-piperazinyl)pyridine-4-boronic acid pinacol ester for compound **10** (see Table 2 for precise structures).

the aim of reducing the PSA to increase CNS penetration because high PSA is well-known to negatively correlate with passive membrane permeability (see Table 2).[17,18] Removal of the pyridyl nitrogen atom (i.e., **8**) had virtually no effect on activity at either enzyme or cellular level. Removal of the piperazine nitrogen atom in addition to the pyridine (i.e., **9**) did not significantly affect activity against *Tb*NMT, although there was a reduction in activity (~10-fold) against the parasite. Although **8** and **9** have reduced PSA compared to **1** (PSA = 79 and 76 Å^2 vs 92 Å^2, respectively), the desired improvement in the brain:blood ratio was not forthcoming with **8**. Capping (alkylating) of the piperazine nitrogen (**10**) caused a noticeable reduction in potency against the parasite.

The Effect of Modifications to the Linker. Previous work[14] had indicated that compounds with an alkyl chain replacing the lower biaryl aromatic linker of **1** had a better degree of selectivity (up to 60-fold) at the enzyme level (see compounds in Figure 4). Therefore, it was decided to

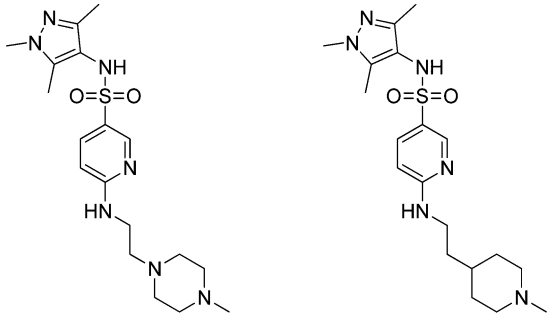

Figure 4. Key compounds as reported previously in ref 14.

investigate modification of the linker. Scheme 3 summarizes the synthetic routes employed to prepare linker-modified compounds **12**–**23**. Compounds **12** and **13** were prepared using the Sonogashira reaction[19] of sulfonamide **7** with 5-

Table 2. Modifications to the Piperazine

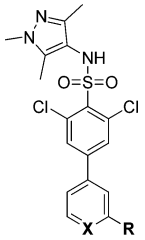

No.	R	*Tb*NMT IC_{50} (μM)[a]	*Hs*NMT IC_{50} (μM)[a]	*T.brucei* EC_{50} (μM)	S	B:B	MRC-5 EC_{50} (μM)
1	X = N 	0.002[b]	0.003	0.002	1.5	< 0.1	0.30
8	X = C 	0.007[b]	0.017	0.006	2.8	< 0.1	0.73
9	X = C 	0.007	0.023	0.023	1.0	nd	1.5
10	X = N 	0.015	0.025	0.020	1.3	nd	0.14

[a]IC_{50} values are shown as mean values of two or more determinations. Standard deviation is typically within 2-fold from the IC_{50}. [b]Compounds with Hill slopes >1.5. *S* = IC_{50} *Hs*NMT/EC_{50} *T. brucei*. B:B is the brain:blood ratio in mouse. nd = not determined.

dx.doi.org/10.1021/jm500809c | J. Med. Chem. 2014, 57, 9855–9869

Scheme 3. Synthesis of Compounds in Table 3[a]

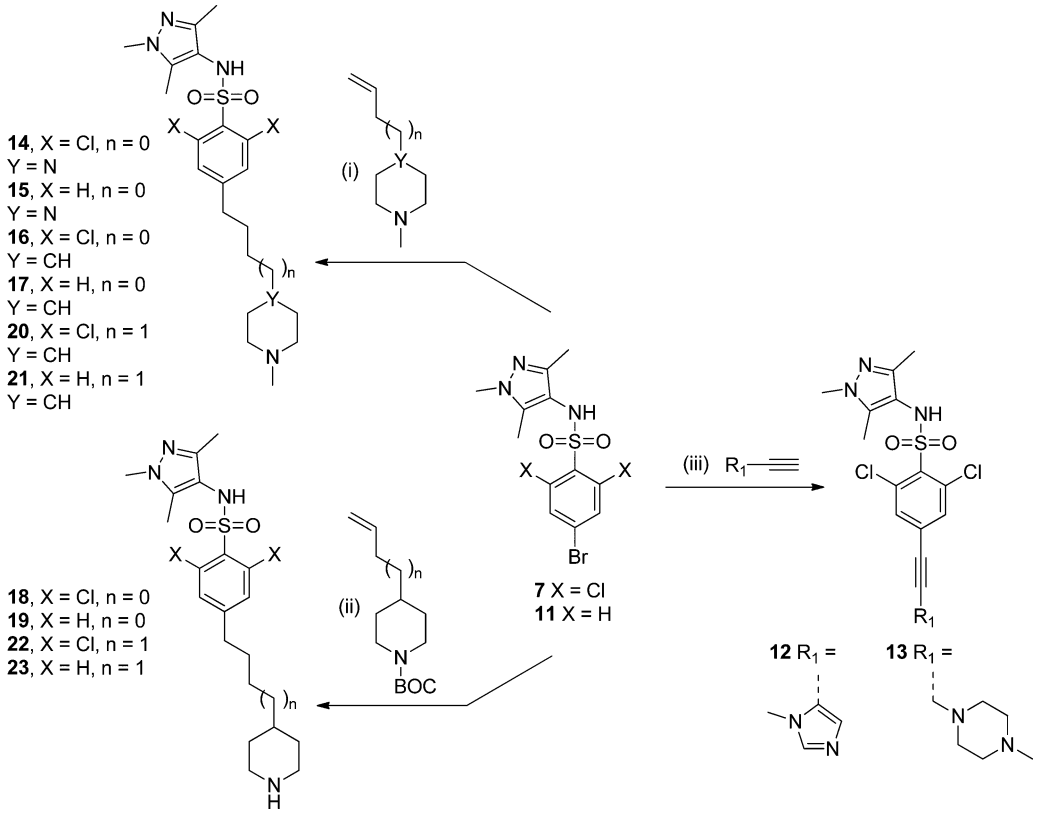

[a](i) Alkene, 9-BBN, THF, 90 °C, then aryl bromide **7** or **11**, $Pd(PPh_3)_4$, K_3PO_4, THF/H_2O; (ii) alkene, 9-BBN, THF, 90 °C, then aryl bromide **7** or **11**, $Pd(PPh_3)_4$, K_3PO_4, THF/H_2O followed by TFA, DCM; (iii) **7**, alkyne, CuI, $Pd(PPh_3)_4$, HN^iPr_2.

ethynyl-1-methyl-*1H*-imidazole and 1-methyl-4-(prop-2-yn-1-yl)piperazine, respectively. In general, sulfonamides **14**–**23**, which bear a pendant amine attached via a saturated alkyl chain, were prepared using a 9-BBN mediated boron-alkyl Suzuki-type coupling reaction[20] between aryl bromide **7** or **11** and the appropriate alkene, i.e. compounds **14**–**17**. Compounds **20** and **21** were prepared by direct addition of the appropriate alkene while secondary amines **18**, **19**, **22**, and **23** were prepared in two steps by coupling with the corresponding BOC-protected alkenes, followed by deprotection with TFA/DCM.

Rigid propargylic systems bearing protonatable tail groups did not have appreciable activity (i.e., **12** and **13**) (see Table 3). Attachment of the terminal piperazine to the aryl core via a flexible propyl linker (i.e., **14**) not only retained reasonable activity but resulted in a marked increase in isoform selectivity (>100-fold) relative to **1**. We cannot rationalize the origin of this selectivity by crystallography, as we do not have structures of the *Tb*NMT and *Hs*NMT complexes. Homology models predict very similar structures in the active sites; therefore, the selectivity may be due to differences in the protein structures remote from the active site, differential protein dynamics[21] or the differential effects of interactions with water in the active site.

The structure of **14** bound to *Af*NMT (Figure 5) confirmed that substitution of the rigid biaryl system with a flexible linker does not alter the binding mode with the piperazine NH interacting with the C-terminal carboxylate via a conserved water molecule, as described for **1**.

Compound **14** was selected as a new lead because, in addition to having significantly improved selectivity ($S = 20$), it was fully curative in a stage 1 mouse model (*T. b. brucei* S427) at a dose of 4 × 50 mg/kg b.i.d. po for 4 days. Work subsequently focused on increasing CNS penetration (brain:-blood ratio of **14** < 0.1) and selectivity of this new framework. Removal of the internal piperazine nitrogen of **14** resulted in a 10-fold improvement in potency (**16**) (EC_{50} = 0.002 μM) and also a small reduction in PSA. Although deletion of this nitrogen appeared to cause a reduction of selectivity at the biochemical level compared to **14** (from >100-fold to approximately 16-fold), comparison of selectivity (S) shows that this modification is selectivity neutral.

Extending the linker by an additional methylene unit (i.e., **20** cf. **16** and **22** cf. **18**) increased activity substantially, resulting in subnanomolar potency against the parasite, although notable gains in selectivity were not achieved with the increased molecular flexibility. Comparison of the structures of **19** and **23** in *Lm*NMT shows that the extra methylene in the linker does not significantly impact the binding mode of the inhibitor (data not shown). Removal of the piperidine *N*-methyl groups of **16** and **20** appeared to reduce potency marginally. Removal of the chlorine atoms from **14**, **16**, **18**, **20**, and **22** consistently reduced potency by at least 10-fold (i.e., **14** vs **15**; **16** vs **17** and **20** vs **21** etc.). Indeed, this appeared to be a general phenomenon within this subseries. The impact of removing the piperidine methyl group on selectivity was greater for the three-carbon linker than the four-carbon linker. Unfortunately, none of the compounds in Table 3 have a brain:blood ratio >0.1 (**14**, **16**, and **17** were tested).

Improving CNS Penetration by "Capping" the Secondary Sulfonamide. It is notable that there are very

dx.doi.org/10.1021/jm500809c | J. Med. Chem. 2014, 57, 9855–9869

Table 3. Modifications to the Linker

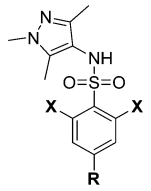

No.	R	X	*Tb*NMT IC_{50} (μM)[a]	*Hs*NMT IC_{50} (μM)[a]	*T.brucei* EC_{50} (μM)	S	MRC-5 EC_{50} (μM)
12	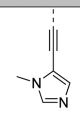	**Cl**	0.66	17	3.9	4.4	16.6
13	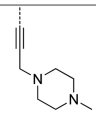	**Cl**	0.16	4.6	0.66	7.0	>50
14	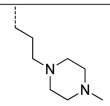	**Cl**	0.003	0.39	0.02	20	31.4
15		**H**	0.12	3.5	0.75	4.7	> 50
16	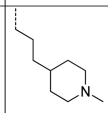	**Cl**	0.002[b]	0.033	0.002	17	2.2
17		**H**	0.007	0.19	0.030	6.3	18.7
18	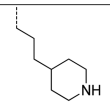	**Cl**	0.002[b]	0.008	0.002	4.0	2.5
19		**H**	0.009	0.13	0.11	1.2	> 50
20	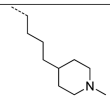	**Cl**	0.001[b]	0.004	0.0005	8.0	0.18
21		**H**	0.003	0.040	0.016	2.5	3.6
22	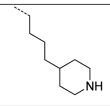	**Cl**	0.003[b]	0.005	0.0006	8.3	0.37
23		**H**	0.006[b]	0.029	0.009	3.2	5.3

[a] IC_{50} values are shown as mean values of two or more determinations. Standard deviation is typically within 2-fold from the IC_{50}. [b] Compounds with Hill slopes >1.5. *S* = IC_{50} *Hs*NMT/EC_{50} *T. brucei*.

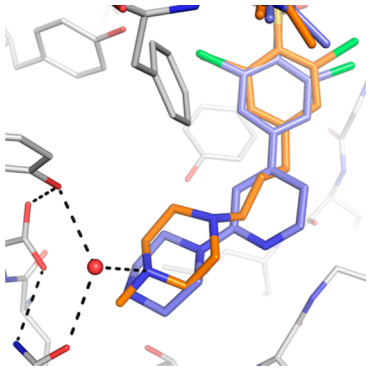

Figure 5. Binding mode of **14** (C atoms gold) bound to *Af*NMT showing the interaction between the piperazine NH and a water molecule coordinated with the C-terminal carboxylate. The binding mode of **1** bound to *Lm*NMT (C atoms slate) is shown for comparison of the piperazine moieties.

few examples of CNS penetrant secondary sulfonamides in the literature.[22−24] The secondary sulfonamide has an appreciable acidity, particularly in compounds where the sulfonyl aromatic bears two halogen atoms (i.e., pK_a of **7** = 6.9 ± 0.5, pK_a of **1** = 7.0 ± 0.5, calculated using ACDlabs software, version 11.02), suggesting the sulfonamide is significantly ionized at physiological pH. Moreover, the secondary sulfonamide exerts a considerable contribution to the overall PSA of compounds in this series (approximately 54 Å^2). Therefore, the sulfonamide was substituted with a variety of capping groups designed to simultaneously reduce PSA and preclude deprotonation of the sulfonamide.

Capping the sulfonamide nitrogen of **7** with a methyl group (i.e., **24**) was found to significantly enhance brain penetration in mice (brain:blood ratio of **7** = <0.1 cf. brain:blood ratio of **24** = 3.7) without unduly affecting potency. Indeed, this modification caused a significant enhancement in CNS penetration across a variety of inhibitors bearing different terminal amines, implicating the sulfonamide moiety as the principal cause of the poor CNS penetration of the parent compounds (see Table 4).

In general, the compounds bearing a tethered amine in Table 4 were prepared via a Suzuki-type reaction[20] with sulfonamides **24**−**28**, which had been modified by *N*-alkylation of sulfonamide **7** (Scheme 4). For instance, compound **40** was prepared by the 9-BBN mediated addition of 4-allyl-1-methylpiperidine with **28**. Notably, we believe this is the first

dx.doi.org/10.1021/jm500809c | *J. Med. Chem.* 2014, 57, 9855−9869

Table 4. Effect on the Brain:Blood Ratio of "Capping" the Sulfonamide with an Alkyl Group

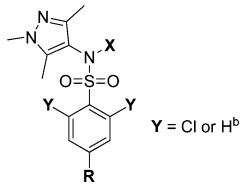

No.	R	X	*Tb*NMT IC_{50} (μM)[a]	*Hs*NMT IC_{50} (μM)[a]	*T.brucei* EC_{50} (μM)	Cl_i[c] (mouse)	B:B	MRC-5 EC_{50} (μM)
7	Br	**H**	0.5	7.3	16	14	< 0.1[c]	>50
24	Br	**Me**	0.33	3.58	5.1	50	3.7[c]	27.2
1	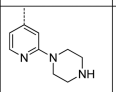	**H**	0.003[d]	0.003	0.002	< 1.0	< 0.1	0.30
29		**Me**	0.002	0.004	0.002	17	0.2	0.14
30[b]		**Me**	0.003	0.022	0.006	1.3	0.2	1.2
31[b]	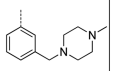	**H**	0.009	0.009	0.043	1.2	0.07	0.79
32[b]		**Me**	0.014	0.017	0.87	9.7	0.3	0.90
14	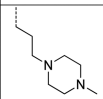	**H**	0.003	0.39	0.023	1.7	< 0.1	31
33		**Me**	0.003	0.19	0.010	7.4	0.6	17
34		**Et**	0.003	0.37	0.016	3.1	1.3	17
35	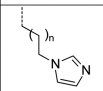	**Me, n = 3**	0.019	0.47	0.22	2.0	nd	21
36		**Me, n = 4**	0.003	0.30	0.026	3.0	1.1	7.8
16		**H**	0.002[d]	0.033	0.002	4.3	< 0.1	2.2
37		**Me**	0.002[d]	0.018	0.001	7.3	0.3	1.1
38[b]		**Me**	0.016	0.39	0.19	3.7	0.4	42
39		**Et**	0.002	0.024	0.003	12	nd	2.2
40		**CHF_2**	0.002[d]	0.012	0.001	2.5	1.6	1.0
41		**CH_2CHF_2**	0.003[d]	0.18	0.013	2.2	nd	3.8
42		**CH_2CF_3**	0.004[d]	0.25	0.011	1.1	0.7	19

[a]IC_{50} values are shown as mean values of two or more determinations. [b]Y = Cl for all compounds except compounds **30**, **31**, **32**, and **38**, where Y = H. [c]The blood:brain ratio was unchanged when measured in wild-type and mdr1a-deficient mice, indicating that neither are Pgp substrates. [d]Compounds with Hill slopes >1.5. [e]Cl_i measured in mL min^{-1} g^{-1}. B:B is the brain:blood ratio in mouse. nd = not determined.

reported application of the difluoromethylation of a secondary sulfonamide, achieved by reaction of **7** with sodium chlorodifluoroacetate.

Methylation of the sulfonamide of lead compound **14** (i.e., **33**) demonstrated that a compound within this series could deliver the desired profile for potency (*Tb*NMT IC_{50} = 0.003 μM, EC_{50} = 0.010 μM), selectivity (*S* = 19), and good brain penetration (brain:blood ratio = 0.6). However, **33** exhibited very poor metabolic stability when incubated with mouse microsomes relative to its parent secondary sulfonamide **14** (Cl_i = 7.4 cf. 1.7 mL/min/g, respectively). While both microsomal stability and CNS exposure could be improved by resorting to the ethyl sulfonamide analogue **34** (brain:blood ratio = 1.3 cf. 0.6; Cl_i = 3.1 cf. 7.4 mL/min/g for **34** and **33**, respectively), microsomal instability was still higher than compound **1**, and this compound had poor oral exposure in mice. Similarly, the more potent piperidine congener of **33**, i.e., **37**, also exhibited a higher microsomal turnover relative to its parent secondary sulfonamide (i.e., compare **37** vs **16**, Cl_i = 7.3 cf. 4.3 mL/min/g, respectively). An hepatic portal vein study in male Sprague–Dawley rat dosed orally with **33** (3 mg/kg) indicated almost total hepatic extraction of the parent (see Figure S2 in Supporting Information), and sulfonamide dealkylation was suspected as the principal mode of elimination. Incubation of compounds **33**, **34**, **37**, and **39** with mouse microsomes, which showed rapid disappearance of parent and the *N*-dealkylated sulfonamide as the predominant metabolite for all compounds, supports this theory (see the metabolite identification study, Table S4 in Supporting Information).

Optimization of the Sulfonamide Capping Group. A variety of compact fluoroalkyl groups were surveyed as sulfonamide caps with the aim of improving metabolic stability and therefore oral exposure (compounds **40** to **42** in Table 4). The 2-fluoroethyl analogue was not included in this study due to its reported potential for conversion to fluoroacetic acid, a metabolic poison.[25] On the basis of higher potency and lower PSA, piperidine **37** instead of **33** was adopted as the test-bed for this investigation.

Replacement of the methyl group of **37** with a 2,2-difluoroethyl group (i.e., **41**) and 2,2,2-trifluoroethyl group (i.e., **42**) successfully resulted in a reduction in microsomal turnover as desired (Cl_i = 7.3, 2.2, and 1.1 mL/min/g, respectively), albeit at the expense of potency, which was reduced approximately 5-fold in both cases. Encouragingly, however, the novel difluoromethylated sulfonamide **40** demonstrated a potency profile similar to the parent compound **37** and had significantly improved stability (i.e., Cl_i 2.5 mL/min/g compared to 7.3 mL/min/g for **37**). In addition to benefiting from greater mouse microsomal stability compared to **33**, **34**, **37**, and **39**, compound **40** did not undergo sulfonamide *N*-dealkylation (see metabolite identification study, Table S4 in Supporting Information). Consistent with greater sulfonamide stability relative to **33**, compound **40** demonstrated good oral exposure in mouse and crucially

dx.doi.org/10.1021/jm500809c | J. Med. Chem. 2014, 57, 9855–9869

Scheme 4. Synthesis of Compounds in Table 4[a]

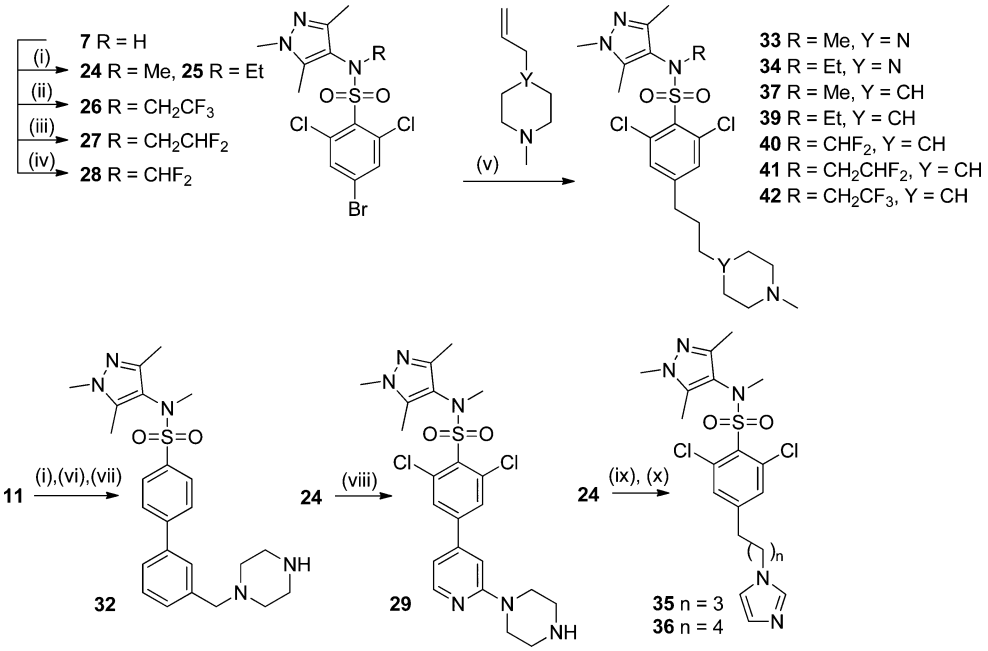

[a](i) NaH, DMF, MeI or EtBr; (ii) CF_3CH_2OMs, K_2CO_3, CH_3CN; (iii) CHF_2CH_2I, K_2CO_3, CH_3CN; (iv) Na^+ $CF_2ClCO_2^-$, K_2CO_3, CH_3CN; (v) alkene, THF, 9-BBN, then aryl bromide **24**–**28**, $Pd(PPh_3)_4$, K_3PO_4, THF/H_2O; (vi) 3-formylphenyl boronic acid, $Pd(PPh_3)_4$, K_3PO_4, THF/H_2O; (vii) piperazine, $NaBH(OAc)_3$, $CHCl_3$; (viii) $Pd(PPh_3)_4$, 2-(1-piperazinyl)pyridine-4-boronic acid pinacol ester, K_3PO_4, THF/H_2O; (ix) pent-4-en-1-ol for compound **35** or hex-5-en-1-ol for compound **36**, THF, 9-BBN, then aryl bromide **24**, $Pd(PPh_3)_4$, K_3PO_4, THF/H_2O; (x) MsCl, NEt_3, pyridine, then imidazole.

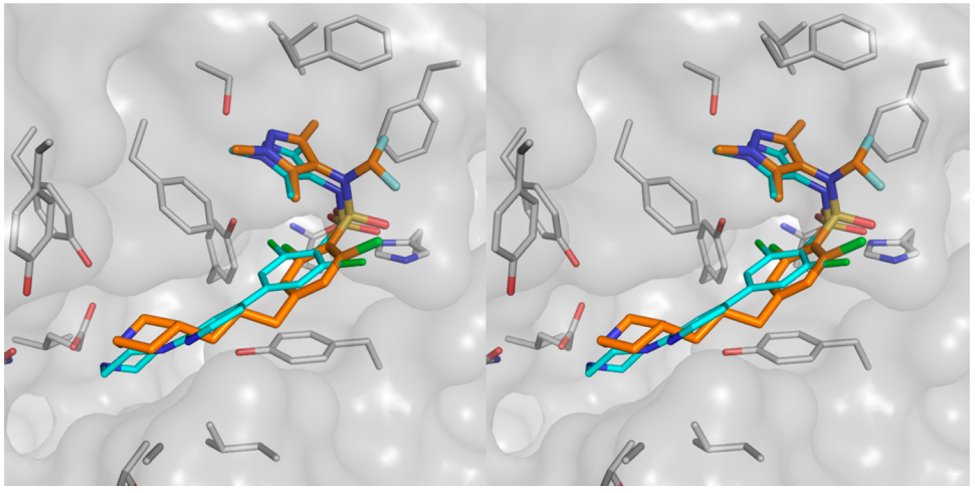

Figure 6. Stereo diagram showing comparison of binding modes of **43** (C atoms gold) and **1** (C atoms cyan) showing retention of sulfonamide configuration after capping with a CHF_2 group.

retained appreciable CNS penetration (brain:blood ratio = 1.6). Unfortunately, some of the compounds described above showed significant inhibition of hERG, which would need further investigation if these compounds were to be progressed (i.e., **40** hERG IC_{50} = 0.6 μM cf. **1** hERG IC_{50} = 28 μM).

Further Optimization of the Linker and Amine on a Tertiary Sulfonamide. Due to its superior potency and improved metabolic stability the difluoromethyl group was retained as the preferred sulfonamide cap in a final study sought to further optimize potency and selectivity of **40** by making modifications in both the tether and the pendant amine portions. The crystal structure of **43** bound to *Af*NMT confirms that the binding mode of the sulfonamide is largely unaffected by capping with the CHF_2 group (see Figure 6).

Compounds were prepared using analogous procedures to those already described according to the conditions shown in Scheme 5. This study resulted in the identification of a large number of highly trypanocidal compounds, some with good CNS penetration (see Table 5 and Table S3, Supporting Information). Unfortunately, however, it proved challenging to obtain substantial selectivity at the enzyme level and there was not an observable trend. Although primary potencies against *Tb*NMT remain substantially unvaried in the low nanomolar range, there is wider variation in activity against the parasite; this is probably a consequence of the inability of the enzyme

dx.doi.org/10.1021/jm500809c | J. Med. Chem. 2014, 57, 9855–9869

Scheme 5. Synthesis of Compounds in Table 5[a]

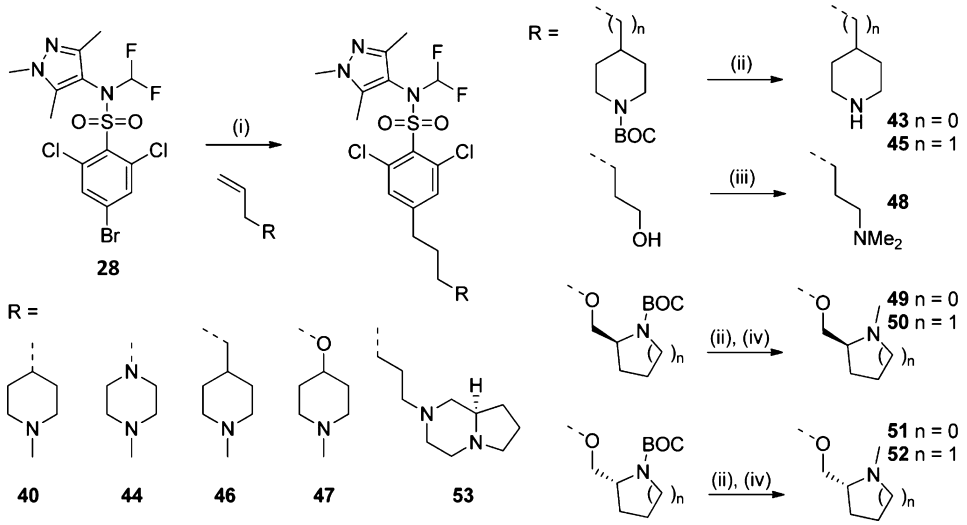

[a](i) Alkene, THF, 9-BBN, 90 °C for 1 h, then sulfonamide **28**, $Pd(PPh_3)_4$ or $Pd(dppf)_2$·DCM, K_3PO_4, THF/H_2O; (ii) TFA, DCM; (iii) MsCl, NEt_3, DCM , then HNMe2, DCM; (iv) Paraformaldehyde, $NaBH(OAc)_3$, $CHCl_3$.

assay to discriminate the most potent compounds due to the tight binding nature of enzyme inhibition (many compounds had high Hill slopes, i.e. ≫ 1).

Key points noted from these studies:

- In the one example for which there is data, converting the terminal tertiary amine to a secondary amine (**40** cf. **43**) caused a large drop in the brain:blood ratio (falls from 1.6 to 0.03).
- Replacement of the piperidine of **40** with a piperazine (i.e., **44**) caused an approximately 10-fold reduction in cellular potency, consistent with previous observations.
- Compound **53**, a bicyclic analogue of **44**, exhibited the best CNS penetration observed within this series (brain:blood ratio = 2.6). However, this compound suffered from high microsomal clearance (Cl_i = 15 mL/min/g) and no improvement to oral exposure in mouse compared to the lead compound **40**.
- An increase in the length of the propyl tether of **40** by an additional methylene (i.e., **46**), or an oxygen atom (i.e., **47**) resulted in similar or slightly better trypanocidal activity while retaining brain:blood ratio.
- Removal of the piperidine ring and replacement by an acyclic linker of comparable length to **46** and **47** was also tolerated (i.e., **48**, *T. brucei* EC_{50} = 0.002 μM). However, these acyclic linkers were very sensitive to the substituents on the terminal amine, with potency decreasing rapidly as the size of substituents on the basic nitrogen is increased (see Table S3 in Supporting Information). While this makes sense intuitively, because the *N*-substituent could potentially impede contact between the basic and acidic centers, it was hoped to strike a potential balance between potency and selectivity by branching into unaccessed space.

It was decided to see if selectivity (*S*) could be improved by the introduction of chiral amines, with substituents which could potentially access different subpockets in the region bound by the terminal amine (see compounds **49**−**53** in Table 5). These modifications resulted in some compounds with subnanomolar potency against *T. brucei* (see Table S3, Supporting Information) and compounds with high selectivity at the biochemical level (i.e., *Hs*NMT/*Tb*NMT is >100-fold for **50**). However, there was no substantial improvement in selectivity (*S*), relative to **40**, with these compounds with the exception of compound **50** (*S* = 47), nor a substantially greater window at the wholly cellular level (i.e., *T. brucei* EC_{50} vs MRC-5) achieved compared with **40**, which already has an approximately 1000-fold differential. Additionally, these compounds generally exhibited higher microsomal intrinsic clearances than **40** and were therefore ruled out of selection for progression into animal models. Comparison of compounds **49**−**52** (i.e., **49** and **50**, cf. **51** and **52**) suggests that the *S*-enantiomers show a marginally greater effect on selectivity (*S*) compared to the *R*-enantiomers.

In addition to those compounds described in Tables 4 and 5, a variety of other amine-bearing cores appended via flexible linkers of varied length to the benzenesulfonamide were evaluated, although none were able to provide the desired profile in terms of potency and selectivity (see Table S3, Supporting Information).

Efficacy in a Stage 2 Model of HAT for "Capped" Sulfonamide Lead Compounds. On the basis of their trypanocidal activity, oral pharmacokinetics, brain:blood ratio, and confirmed fully curative activity in the stage 1 mouse model (*T. b. brucei* S427, 50 mg/kg b.i.d. po for 4 days), compounds **40**, **46**, and **42** were selected for evaluation in the stage 2 mouse model of HAT (*T. b. brucei* GVR35). With the assumption that the brain interstitial fluid is the biophase for effective cure of stage 2 HAT and that EC_{99} drug levels are required,[15] it was calculated (using *T. b. brucei* S427 EC_{50}, mouse oral pharmacokinetics, measured brain total concentration, and brain free fraction) that an oral dose of 20 mg/kg b.i.d., 15 mg/kg b.i.d., or 250 mg/kg b.i.d. for **40**, **46**, and **42**, respectively would be needed to deliver stage 2 cures based on maintaining the brain free concentration (as a surrogate of brain interstitial fluid levels[26]) above the *T. brucei* EC_{99} (see Table S5, Supporting Information for dose calculations). All the compounds were dosed in the stage 2 mouse model of HAT (*T. b. brucei* GVR35) at the MTD (100, 50, or 150 mg/kg b.i.d. po for **40**, **46**, and **42**, respectively) for 5 days. However, some

dx.doi.org/10.1021/jm500809c | J. Med. Chem. 2014, 57, 9855−9869

Table 5. Optimization of the Linker and the Terminal Amine of a CHF_2-Capped Sulfonamide

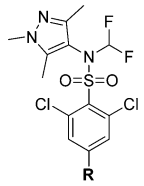

No.		*Tb*NMT IC_{50} (μM)[a]	*Hs*NMT IC_{50} (μM)[a]	*T.brucei* EC_{50} (μM)	Cl_i[d] (mouse)	B:B	S	MRC-5 EC_{50} (μM)
40 X = Me		0.002[b]	0.012	0.001	2.5	1.6	12	1.00
43 X = H		0.003[b]	0.009	0.003	0.8	0.03	3	0.51
44	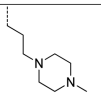	0.003[b]	0.16	0.010	4.2	nd	16	7.2
45 X = H		0.003[b]	0.004	0.001	1.0	nd	4.0	0.11
46 X = Me		0.002[b]	0.005	0.0006	1.3	1.3	8.3	0.20
47	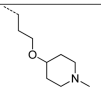	0.002[b]	0.005	0.0006	3.7	0.9	8.3	0.16
48[c]	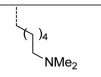	0.002[b]	0.008	0.002	3.7	nd	4.0	0.65
49	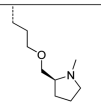	0.002[b]	0.074	0.004	8.7	nd	19	2.8
50	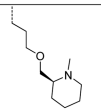	0.002[b]	0.28	0.006	9.8	nd	47	3.9
51	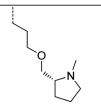	0.002	0.045	0.004	nd	nd	11	3.2
52	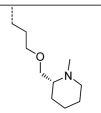	0.002[b]	0.15	0.013	14.2	nd	12	3.5
53	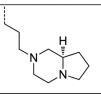	0.002[b]	0.047	0.005	15	2.6	9.4	3.1

[a] IC_{50} values are shown as mean values of two or more determinations. [b] Compounds with Hill slopes >1.5. [c] For analogues where the size of the *N*-substituent was varied, see Table S3 in Supporting Information. [d] Cl_i measured in mL min^{-1} g^{-1}. B:B is the brain:blood ratio in mouse. *S* = IC_{50} *Hs*NMT/EC_{50} *T. brucei*. nd = not determined.

toxicity was observed at this dose regimen in infected mice for both **40** (1/5 mice) and **46** (2/5 mice). Although **42** was well tolerated, none of the mice were cured, which was somewhat expected based on the above calculation. For **40** and **46**, further dosing regimens were tested in order to try and achieve in vivo proof-of-concept in a stage 2 HAT model (**40**: 50 mg/kg b.i.d. po for 10 days, 100 mg/kg b.i.d. po for 8 days, and three rounds of 3 day dosing at 100 mg/kg with a two day "drug holiday" between rounds. **46**: 25 mg/kg b.i.d. for 10 days, 50 mg/kg b.i.d. po for 8 days). Encouragingly, the two 100 mg/kg extended dosing schedules for **40** were partially efficacious (1/5 mice). However, no cures were achieved at 50 mg/kg b.i.d. po for 10 days with either dose regimen of **46**. Indeed, significant toxicity was observed for the extended 50 mg/kg dose regimen of **46**. Kaplan−Meier graphs for efficacy of compound **40** in continuous and pulsed dosing regimens are shown in Figure 7.

Although this outcome is encouraging for **40**, it was disappointing that full cures were not achieved considering a 20 mg/kg b.i.d. oral dose was predicted to be efficacious. A possible explanation for this is the difference observed in minimal curative efficacy to different parasite strains, as has already been seen for key NMT compounds. For example, an efficacy study of compound **46** showed approximately a 4-fold reduction in efficacy in an acute model of *T. b. brucei* GVR35 (minimum curative dose 25 mg/kg b.i.d. po for 4 days) compared to *T. b. brucei* S427 (minimum curative dose 6 mg/kg b.i.d., po for 4 days). The predicted efficacy of **40** was based on *T. b. brucei* S427 data, and if efficacy to *T. b. brucei* GVR35 is

dx.doi.org/10.1021/jm500809c | *J. Med. Chem.* 2014, 57, 9855−9869

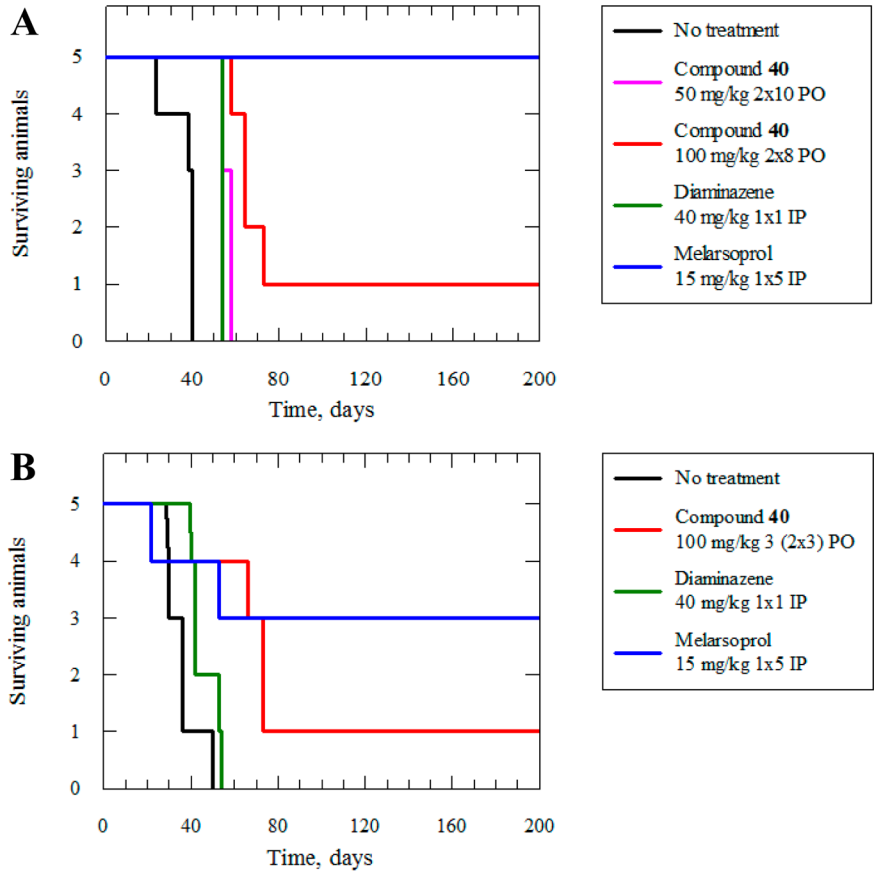

Figure 7. Kaplan–Meier survival graph for compound **40** in the *T. b. brucei* GVR35 stage 2 HAT efficacy model ((A) continuous; (B) pulsed dosing).

4–5-fold less sensitive (not tested), as was observed for **46**, a 100 mg/kg b.i.d. po dose regimen of **40** would be on the cusp of efficacy. It was therefore unfortunate that a lack of tolerability prevented higher dosing to deliver full cures. While compounds **49** and **50** have better selectivity (*S*) than **40** and may therefore be better tolerated at a higher dose required for efficacy, their high metabolic instability ruled them out from further evaluation.

CONCLUSIONS

In this article, we describe optimization of the lead pyrazole sulfonamide **1** which resulted in compound **40**, which has markedly increased blood–brain barrier penetration and improved selectivity. We have a more complete understanding of the SAR of this series and how to achieve blood–brain barrier penetration by capping the sulfonamide group which reduces the PSA and acidity. While a greater degree of selectivity has also been obtained, achieved through introduction of a flexible linker between the pyrazole and amine, the reasons for this are not fully understood. It is important to note that the downside of these modifications to **1** is a significant increase in lipophilicity (cLogP of **1** and **40** is 3.1 and 4.7 respectively), which, when combined with a reduction in PSA, potentially increases the risk of off-target activity.[27] This may be the cause of the poor tolerability of compound **40**.

Evaluation of key tool compounds from this series in a CNS model of HAT resulted in partial efficacy. Lack of full cure is likely to be a consequence of insufficient therapeutic window to be able to deliver fully efficacious free drug concentration to the brain at a tolerated dose, further confounded by the lower efficacy of these compounds toward the *T. b. brucei* GVR35 strain compared to the *T. b. brucei* S427 strain. Compounds with better selectivity would hopefully allow dosing at either higher levels or for longer duration and therefore result in a fully curative stage 2 *Tb*NMT lead. It is, however, encouraging that some cures and prolongation of survival in the stage 2 model is observed via blockade of *Tb*NMT because this increases confidence in the validity of this target for the development of therapeutics for stage 2 HAT. The compounds described above, including compound **40**, and the increased understanding of how to optimize compounds for both BBB penetration and selectivity represent a very useful platform for further studies.

EXPERIMENTAL SECTION

General Experimental Information. Chemicals and solvents were purchased from the Aldrich Chemical Co., Fluka, ABCR, VWR, Acros, Fisher Chemicals, and Alfa Aesar and were used as received unless otherwise stated. Air- and moisture-sensitive reactions were carried out under an inert atmosphere of argon in oven-dried glassware. Analytical thin-layer chromatography (TLC) was performed on precoated TLC plates (layer 0.20 mm silica gel 60 with fluorescent indicator UV254, from Merck). Developed plates were air-dried and analyzed under a UV lamp (UV254/365 nm). Flash column chromatography was performed using prepacked silica gel cartridges (230–400 mesh, 40–63 μm, from SiliCycle) using a Teledyne ISCO Combiflash Companion or Combiflash Retrieve. ^{1}H NMR, ^{13}C NMR, ^{19}F NMR, and 2D-NMR spectra were recorded on a Bruker Avance DPX 500 spectrometer (^{1}H at 500.1 MHz, ^{13}C at 125.8 MHz, ^{19}F at 470.5 MHz). Chemical shifts (δ) are expressed in ppm recorded using

dx.doi.org/10.1021/jm500809c | J. Med. Chem. 2014, 57, 9855–9869

the residual solvent as the internal reference in all cases. Signal splitting patterns are described as singlet (s), doublet (d), triplet (t), quartet (q), multiplet (m), broad (b), or a combination thereof. Coupling constants (J) are quoted to the nearest 0.1 Hz. LC-MS analyses were performed with either an Agilent HPLC 1100 series connected to a Bruker Daltonics MicrOTOF or an Agilent Technologies 1200 series HPLC connected to an Agilent Technologies 6130 quadrupole LC/MS, where both instruments were connected to an Agilent diode array detector. LC−MS chromatographic separations were conducted with a Waters Xbridge C18 column, 50 mm × 2.1 mm, 3.5 μm particle size; mobile phase, water/acetonitrile + 0.1% HCOOH, or water/acetonitrile +0.1% NH_3; linear gradient from 80:20 to 5:95 over 3.5 min and then held for 1.5 min; flow rate of 0.5 mL min^{-1}. All assay compounds had a measured purity of ≥95% (by TIC and UV) as determined using this analytical LC−MS system. High resolution electrospray measurements were performed on a Bruker Daltonics MicrOTOF mass spectrometer. Microwave-assisted chemistry was performed using a Biotage Initiator Microwave Synthesizer.

*Prototypical Procedure for the Suzuki Reaction between an Aryl Bromide and a Boronic Acid/Boronate Ester: 2,6-Dichloro-4-(2-piperazin-1-yl-pyridin-4-yl)-N-(1,3,5-trimethyl-1H-pyrazol-4-yl)-benzenesulfonamide (**1**).* A deoxygenated solution of 4-bromo-2,6-dichloro-*N*-(1,3,5-trimethyl-1*H*-pyrazol-4-yl)-benzenesulfonamide (13.84 g, 33.3 mmol), 2-(1-piperazinyl)pyridine-4-boronic acid pinacol ester (11.57 g, 40.0 mmol), K_3PO_4 (9.73 g, 44.0 mmol), and $Pd(PPh_3)_4$ (1.50 g, 0.96 mmol) in DMF (200 mL) and water (40 mL) in a round-bottomed flask under argon was heated at 120 °C for 1 h. The reaction mixture was then concentrated in vacuo, diluted with DCM (400 mL), washed with saturated aqueous ammonia solution (2 × 100 mL), dried ($MgSO_4$), and concentrated in vacuo. The residual solid was triturated from Et_2O and collected by filtration to give a solid, which was recrystallized from EtOAc to give the title compound **1** as an off-white powder (15.22 g, 30.7 mmol, 92%). ^{1}H NMR (500 MHz, DMSO-d_6): δ 9.79 (s, 1H), 8.25 (d, J = 5.9 Hz, 1H), 8.20 (s, 2H), 7.61 (s, 1H), 7.40 (d, J = 5.9 Hz, 1H), 4.08 (s br, 4H), 3.63 (s, 3H), 3.28 (s br, 4H), 2.00 (s, 3H), 1.77 (s, 3H). ^{13}C NMR (125 MHz, DMSO-d_6): 147.5, 147.3, 143.8, 137.4, 136.3, 135.2, 129.8, 111.8, 111.7, 109.1, 108.9, 42.7, 42.0, 36.2, 10.4. HRMS (m/z): $[M + H]^+$ calcd for $C_{21}H_{25}N_6SO_2Cl_2$, 495.1131; found, 495.1124.

*Prototypical Procedure for Preparation of a Sulfonamide from an Amine and a Sulfonyl Chloride: 4-Bromo-N-(1,3,5-trimethyl-1H-pyrazol-4-yl)-benzenesulfonamide (**11**).* 4-Bromobenzenesulfonyl chloride (5.0 g, 19.6 mmol) was added portionwise to a stirred solution of 4-amino-1,3,5-trimethyl-1*H*-pyrazole (2.45 g, 19.6 mmol) in pyridine (50 mL) at rt. The reaction was stirred for 24 h then concentrated to dryness in vacuo. The resulting residue was diluted with DCM (100 mL), washed with aqueous sodium hydroxide solution (0.5M, 100 mL), organic phase separated, dried ($MgSO_4$), filtered, and concentrated to dryness in vacuo. Trituration from Et_2O and collection by vacuum filtration gave the title compound **11** as a fine off-white solid (5.1 g, 14.8 mmol, 79%). ^{1}H NMR (500 MHz, DMSO-d_6): δ 9.21 (1H, s), 7.79 (d, J = 8.5 Hz, 2H), 7.56 (d, J = 8.5 Hz, 2H), 3.56 (s, 3H), 1.82 (s, 3H), 1.61 (s, 3H). HRMS (m/z): $[M + H]^+$ calcd for $C_{12}H_{15}N_3SO_2Br$, 344.0063; found, 344.0059.

*Prototypical Procedure for N-Alkylation of a Sulfonamide with an Alkyl Halide: 4-Bromo-N-methyl-N-(1,3,5-trimethyl-1H-pyrazol-4-yl)-benzenesulfonamide (**24**).* Sodium hydride (95% w/w, 88 mg, 3.48 mmol) was added portionwise to a solution of 4-bromo-*N*-(1,3,5-trimethyl-1*H*-pyrazol-4-yl)-benzenesulfonamide (1.0 g, 2.91 mmol) in DMF (10.0 mL) at 0 °C. When effervescence had ceased, methyl iodide (217 μL, 3.48 mmol) was added dropwise and the reaction was allowed to warm to rt over 4 h. The reaction was concentrated to dryness in vacuo, diluted by addition of DCM (30 mL), washed with water (2 × 15 mL), dried ($MgSO_4$), and concentrated in vacuo. The residue was triturated from Et_2O and collected by vacuum filtration to give the title compound **24** as a fine off-white solid (557 mg, 1.56 mmol, 54%). ^{1}H NMR (500 MHz, DMSO-d_6): δ 9.67 (s, 1H), 8.78 (d, J = 5.7 Hz, 1H), 8.51 (d, J = 8.6 Hz, 1H), 8.09 (d, J = 5.8 Hz, 1H), 7.86 (d, J = 5.6 Hz, 1H), 7.50 (d, J = 5.7 Hz, 1H), 7.21 (d, J = 8.4 Hz, 2H), 4.17 (d, J = 8.4 Hz, 2H), 4.34 (s, 1H), 4.18−4.14 (m, 1H), 3.21 (dd, J = 4.9 Hz 13.9 Hz, 1H) 2.98 (dd, J = 9.3 Hz 13.9 Hz, 1H), 1.06 (s, 3H), 0.99 (s, 3H). m/z (ES^+, 70 V) 404.1 (MH^+).

*4-Bromo-2,6-dichloro-N-(difluoromethyl)-N-(1,3,5-trimethyl-1H-pyrazol-4-yl)benzenesulfonamide (**28**).* A well-stirred slurry of 4-bromo-2,6-dichloro-*N*-(1,3,5-trimethyl-1*H*-pyrazol-4-yl)-benzenesulfonamide (3.0 g, 7.2 mmol), potassium carbonate (3.0 g, 21.0 mmol), and sodium chlorodifluoroacetate (3.3 g, 21.0 mmol) in acetonitrile (100.0 mL) was heated to 60 °C for 48 h. The resulting slurry was then concentrated in vacuo, diluted with DCM (100 mL) and water (100 mL), the organic phase separated, dried ($MgSO_4$), and concentrated in vacuo. Trituration of the residue with diethyl ether gave a precipitate, which was collected by vacuum filtration and dried to give the title compound **28** as a fine white powder (2.05 g, 4.43 mmol, 62%). ^{1}H NMR (500 MHz, $CDCl_3$): δ 7.61 (2H, s), 7.34 (1H, dd, J = 59.4 Hz 61.2 Hz), 3.67 (3H, s), 2.01 (3H, s), 1.71 (3H, s). m/z (ES^+, 70 V) 464.1 (MH^+).

*Prototypical Procedure for Coupling of an Aryl Bromide with a 9-BBN-Derived Trialkylborane under B-Alkyl Suzuki−Miyaura Conditions: 2,6-Dichloro-N-(difluoromethyl)-4-(3-(1-methylpiperidin-4-yl)propyl)-N-(1,3,5-trimethyl-1H-pyrazol-4-yl)benzenesulfonamide (**40**).* A solution of 4-allyl-1-methylpiperidine (776 mg, 5.54 mmol) in THF (10.0 mL) under nitrogen at rt was treated dropwise with 9-BBN (0.5 M in THF, 13.2 mL, 6.6 mmol). The reaction was then heated in a microwave for 30 min at 90 °C. The resulting solution was then reduced to approximately half its original volume by passage of nitrogen then transferred via cannula into a stirred mixture of **28** (2.5 g, 5.4 mmol) and K_3PO_4 (1.27 g, 6.0 mmol) in DMF (10.0 mL) and water (2.0 mL) under argon. After bubbling argon through the reaction for 5 min at rt, $Pd(PPh_3)_4$ (160 mg, 0.14 mmol) was added and the reaction vessel sealed and then heated in a microwave at 80 °C for 30 min. The cooled reaction mixture was then concentrated in vacuo, diluted with DCM (50 mL) and aqueous ammonia solution (50 mL), and the organic phase separated, washed with brine (2 × 25 mL), dried ($MgSO_4$), and concentrated in vacuo. Chromatography (SiO_2, EtOAc:MeOH:saturated aqueous ammonia solution 10:1:0.1) gave the title compound **40** as a white powder (2.41 g, 4.6 mmol, 85%). ^{1}H NMR (500 MHz, DMSO-d_6): δ 7.69 (t, J = 60.3 Hz, 1H), 7.62 (s, 2H), 3.63 (s, 3H), 3.35 (s br, 2H), 2.90−2.80 (m, 2H), 2.67 (s, 3H), 2.63 (t, J = 7.4 Hz, 2H), 1.86 (s, 3H), 1.84−1.77 (m, 2H), 1.62 (s, 3H), 1.60−1.55 (m, 2H), 1.49−1.32 (m, 3H), 1.20−1.13 (m, 2H). HRMS (m/z): $[M + H]^+$ calcd for $C_{22}H_{31}N_4SO_2Cl_2F_2$, 523.1507; found, 523.1490. ^{13}C NMR (125 MHz, DMSO-d_6): δ 151.1, 145.9, 140.3, 135.2, 132.0, 129.5, 111.1, 105.9, 53.3, 42.5, 36.5, 34.6, 33.8, 32.3, 28.9, 26.8, 10.2, 8.6. ^{19}F NMR (470 MHz, DMSO-d_6): δ −92.2 (dd, J = 60.3 Hz 207.8 Hz, 1F), −94.4 (dd, J = 60.3 Hz 207.5 Hz, 1F), spectrum was not ^{1}H-decoupled.

Enzyme Inhibition Assay. *N*-Myristoyltransferase is an enzyme that catalyzes the addition of myristic acid from myristoyl-CoA to the N-terminal glycine residue of numerous substrate proteins and peptides with the subsequent release of coenzyme A. ^{3}H-labeled myristoyl-CoA (GE Healthcare) can be used in the reaction to transfer ^{3}H-myristic acid to a biotinylated substrate peptide (GCGGSKVKPQPPQAK(biotin)-amide, Pepceuticals Inc.). The reaction can be measured by the subsequent binding of the labeled peptide to streptavidin-coated scintillation proximity assay (SPA) beads (GE Healthcare) and monitoring of β-particle excitation of the embedded scintillant. Measurement of the ability of compounds to inhibit the *N*-myristoyltransferase enzyme(s) of human (*Hs*NMT-1 and *Hs*NMT-2) and kinetoplast (*T. brucei*, *T. cruzi*, and *L. major*) species was performed using a modification of the scintillation proximity assay platform described previously by Panethymitaki et al.[28] as follows: Compounds were solubilized in DMSO at a top concentration of 10 mM and serially diluted in half log steps to achieve a range of final assay concentrations of 100 μM to 1.5 nM. Compound at each concentration was added to white 384-well plates in a volume of 0.5 μL. *N*-Myristoyltransferase enzyme (*Hs*NMT-1, *Hs*NMT-2, *Tc*NMT, *Tb*NMT, or *Lm*NMT), dissolved to a working concentration of 10 nM in assay buffer (30 mM Tris-HCl, pH 7.4, 0.5 mM EGTA, 0.5 mM EDTA, 1.25 mM DTT, 0.1% Triton X-100), was then added to columns 1−11 and 13−23 of the plates in a volume of

20 μL. To columns 12 and 24, 20 μL of assay buffer was added to provide a no-enzyme control. Following a 5 min incubation at room temperature, the substrates (GCGGSKVKPQPPQAK(biotin)-amide and myristoyl-CoA), dissolved in assay buffer, were added to all wells in a volume of 20 μL to start the reaction. The final concentrations of peptide and ^{3}H-myristoyl-CoA were 0.5 μM and 125 nM, respectively, and the specific activity of the radiolabel was 8 Ci/mmol. Plates were then incubated at room temperature for up to 50 min (dependent upon the period of linearity for the different enzyme species) before SPA beads, suspended to 1 mg/mL in a stop solution (200 mM phosphoric acid/NaOH, pH 4, 750 mM $MgCl_2$), were added in a volume of 40 μL. Plates were then read on a TopCount microplate luminometer and data analyzed by calculating the percentage inhibition compared to the maximum and minimum assay controls. Concentration effect curves were fitted using nonlinear regression using XLFit 4.2, and IC_{50} values were determined.

Cell Viability Assay. Measurement of the ability of the compounds to inhibit human (MRC5, human lung fibroblast cells) and trypanosome (*T. b. brucei*, BSF427, VSG118) cell growth was performed using a modification of the cell viability assay previously described by Raz et al.[29] Compounds were dissolved in DMSO at a top concentration of 10 mM and serially diluted in half log steps to achieve a range of final assay concentrations of 50 μM to 0.5 nM. Compound at each concentration (200-fold final) was added to clear 96-well tissue culture plates in a volume of 1 μL. Then 2000 cells per well in relevant growth medium (HMI-9T for *T. brucei*, a modification of HMI-9 as described by Hurumi et al.,[30] where 0.2 mM 2-mercaptoethanol was replaced with 0.056 mM thiolglycerol, and MEM with 10% FBS for MRC-5) were then added to columns 1−11 of the plates in a volume of 199 μL. To column 12, 200 μL of medium was added to provide a no cells control. Plates were then incubated at 37 °C in an atmosphere of 5% CO_2 for 69 h before the addition of 20 μL of 500 μM rezasurin solution and a further incubation period of 4 h. Plates were then read on a BioTek flx800 fluorescent plate reader, and percentage inhibition was compared to the maximum and minimum assay controls. Concentration effect curves were fitted using nonlinear regression using XLFit 4.2 and EC_{50} values determined.

Protein Crystallization and Structure Determination. Detailed descriptions of protein expression, crystallization, and structure determination for *Af*NMT complexes will be reported in a separate manuscript (Fang et al., manuscript submitted). Ternary complexes of *Af*NMT with myristoyl CoA (MCoA) and ligands of interest were obtained by cocrystallization by incubating protein with 10 mM MCoA plus 10 mM ligand diluted from a 100 mM stock in DMSO prior to crystallization. Coordinates and associated diffraction data for complexes of *Af*NMT + compounds **14** and **43** have been deposited in the Protein Data Bank (PDB) with accession codes 4UWI and 4UWJ, respectively. Data measurement and refinement statistics are shown in Table S6 (Supporting Information).

Intrinsic Clearance (Cl_i) Experiments. Test compound (0.5 μM) was incubated with female CD1 mouse liver microsomes (Xenotech LLC ; 0.5 mg/mL 50 mM potassium phosphate buffer, pH7.4) and the reaction started with addition of excess NADPH (8 mg/mL 50 mM potassium phosphate buffer, pH 7.4). Immediately, at time zero, then at 3, 6, 9, 15, and 30 min, an aliquot (50 uL) of the incubation mixture was removed and mixed with acetonitrile (100 uL) to stop the reaction. Internal standard was added to all samples, the samples centrifuged to sediment precipitated protein, and the plates then sealed prior to UPLC-MS/MS analysis using a Quattro Premier XE (Waters corporation, USA).

XLfit (IDBS, UK) was used to calculate the exponential decay and consequently the rate constant (k) from the ratio of peak area of test compound to internal standard at each time point. The rate of intrinsic clearance (Cl_i) of each test compound was then calculated using the equation Cli (mL/min/g liver) = $k \times V \times$ microsomal protein yield, where V (mL/mg protein) is the incubation volume/mg protein added and microsomal protein yield is taken as 52.5 mg protein/g liver. Verapamil (0.5 μM) was used as a positive control to confirm acceptable assay performance.

Mouse Pharmacokinetics. Test compound was dosed as a bolus solution intravenously at 3 mg free base/kg (dose volume, 5 mL/kg; dose vehicle, saline or 5% DMSO; 40% PEG400; 55% saline) to female NMRI mice (n = 3) or dosed orally by gavage as a solution at 10 and/or 50 mg free base/kg (dose volume, 5 mL/kg; dose vehicle, 5% DMSO; 95% distilled water or 5% DMSO; 40% PEG400; 55% distilled water) to female NMRI mice (n = 3/dose level). Female NMRI mice were chosen as these represent the sex and strain used for the stage 1 and stage 2 HAT efficacy models. Blood samples were taken from each mouse at 2 (IV only), 5 (IV only), 15, and 30 min, 1, 2, 4, 6, 8, and 24 (po only) hours postdose and mixed with two volumes of distilled water. After suitable sample preparation, the concentration of test compound in blood was determined by UPLC-MS/MS using a Quattro Premier XE (Waters, USA). Pharmacokinetic parameters were derived from the mean blood concentration time curve using PKsolutions software v 2.0 (Summit Research Services, USA).

Mouse Brain Penetration. Each compound was dosed as a bolus solution intravenously at 2 mg free base/kg (dose volume, 5 mL/kg; dose vehicle, 5% DMSO; 95% saline) to female NMRI mice (n = 6). At 5 and 30 min following intravenous bolus injection of test compound, mice (n = 3/time point) were placed under terminal anesthesia with isofluorane. A blood sample was taken by cardiac puncture into two volumes of distilled water and the brain removed. After suitable sample preparation, the concentration of test compound in blood and brain was determined by UPLC-MS/MS using a Quattro Premier XE (Waters, USA). For each mouse at each time point, the concentration in brain (ng/g) was divided by the concentration in blood (ng/mL) to give a brain:blood ratio. The mean value obtained was quoted.

Efficacy Experiments. Stage 1 efficacy experiments using *T. b. brucei* S427 were performed according to methods described by Frearson et al.[15]

T. b. brucei GVR35 Stage 2 Efficacy Protocol. NMRI mice used in the experiment were purchased from Harlan, UK. Mice were maintained under standard temperature/lighting conditions and given food and water ad libitum. The trypanosomes used in this study were of the cloned stabilate *T. b. brucei* GVR35, originally derived from trypanosomes isolated from a wildebeest in the Serengeti in 1966.[31] By 13 days postinfection, parasites entered the CNS.[32] If treatment is delayed until 21 days after infection, successful cure is therefore dependent on the ability of the compound to penetrate through the blood−brain barrier.[33] This model is widely used to evaluate the efficacy of new compounds for treatment against stage 2 HAT.[34]

Cryopreserved *T. b. brucei* GVR35 trypomastigotes were diluted to ∼5 × 10^4 cells/mL in 20 mM Hanks Balanced Salt Solution with glucose, and 0.2 mL of that dilution was used for infection (∼1 × 10^4 cells/mL per animal). All animals in the groups were intraperitoneally infected (ip) on day 0. After infection, parasitaemia was monitored by examination of tail blood smears. On day 21, post infection animals were randomly allocated to five mice per group. Infected animals were dosed with one of the following: diaminazene diaceturate (ip), 40 mg/kg once only as a HAT stage 1 control (early stage tyrypanocide to clear the parasites in the systemic circulation and in tissues other than CNS); Melasoprol (ip), 10 mg/kg once daily for 5 days as a positive control for HAT stage 2; or test compound (gavage) twice daily for 10 days (i.e., **40**, **42**, or **46**) or twice daily for 3 × 3 days with 2 days rest between dose intervals (i.e., **40**). One group of five mice was an untreated control group. The dose solutions were prepared daily, using 5% DMSO:40% PEG400:55% Milli-Q water for compound (i.e., **40**) and 10% DMSO:90% peanut oil for control drugs. To measure the response to treatment, parasitaemia was monitored twice per week until day 50. After day 50, the mice were checked only once per week until day 180 post treatment. Mice surviving to the end of experiment and blood smear aparasitaemic were considered cured.

All regulated procedures on living animals were carried out under the authority of licenses issued by the Home Office under the Animals (Scientific Procedures) Act 1986, as amended in 2012 (and in compliance with EU Directive EU/2010/63). License applications

were approved by the University's Ethical Review Committee (ERC) before submission to the Home Office.

■ ASSOCIATED CONTENT

Supporting Information

Synthetic details for all compounds, supplementary data tables, additional information on ADMET and pharmacology, and crystallographic data tables. This material is available free of charge via the Internet at http://pubs.acs.org.

Accession Codes

Coordinates and associated diffraction data for complexes of *Af*NMT with compounds **14** and **43** have been deposited in the Protein Data Bank (PDB) with accession codes 4UWI and 4UWJ, respectively.

■ AUTHOR INFORMATION

Corresponding Authors

*For I.H.G.: phone, +44 1382 386 240; E-mail, i.h.gilbert@dundee.ac.uk.

*For K.D.R.: phone, +44 1382 388 688; E-mail, k.read@dundee.ac.uk.

Notes

The authors declare no competing financial interest.

■ ACKNOWLEDGMENTS

Funding for this work was provided by the Wellcome Trust (grants WT077705, WT083481, WT085622). We thank Gina MacKay for performing HRMS analyses and for assistance with performing other NMR and MS analyses, Daniel James for data management, Bhavya Rao for performing parasite assays, Dhananjay Joshi and Mary Gardiner for performing enzyme assays, and Dr. Stephen Patterson for critical evaluation of the manuscript.

■ ABBREVIATIONS USED

B:B, brain to blood ratio; 9-BBN, 9-borabicyclo(3.3.1)nonane; Cl_i, intrinsic clearance; EC_{99}, 99% of maximal effective concentration; GVR35, Glasgow Veterinary Research-35 strain; HAT, human African trypanosomiasis; MRC-5, Medical Research Council-5; NMT, *N*-myristoyltranferase; NMRI, Naval Medical Research Institute; STIB900, Swiss Tropical Institute, Basel-900 strain

■ REFERENCES

(1) Brun, R.; Don, R.; Jacobs, R. T.; Wang, M. Z.; Barrett, M. P. Development of novel drugs for human African trypanosomiasis. *Future Microbiol.* **2011**, *6*, 677−691.

(2) Stuart, K. D.; Brun, R.; Croft, S. L.; Fairlamb, A.; Gurtler, R. E.; McKerrow, J. H.; Reed, S.; Tarleton, R. Kinetoplastids: related protozoan pathogens, different diseases. *J. Clin. Invest.* **2008**, *118*, 1301−1310.

(3) Jacobs, R. T.; Nare, B.; Phillips, M. A. State of the Art in African Trypanosome Drug Discovery. *Curr. Top. Med. Chem.* **2011**, *11*, 1255−1274.

(4) Farazi, T. A.; Waksman, G.; Gordon, J. I. The biology and enzymology of protein *N*-myristoylation. *J. Biol. Chem.* **2001**, *276*, 39501−39504.

(5) Resh, M. D. Trafficking and signaling by fatty-acylated and prenylated proteins. *Nature Chem. Biol.* **2006**, *2*, 584−590.

(6) Rudnick, D. A.; McWherter, C. A.; Rocque, W. J.; Lennon, P. J.; Getman, D. P.; Gordon, J. I. Kinetic and structural evidence for a sequential ordered Bi Bi mechanism of catalysis by *Saccharomyces cerevisiae* myristoyl-CoA:protein *N*-myristoyltransferase. *J. Biol. Chem.* **1991**, *266*, 9732−9739.

(7) Price, H. P.; Menon, M. R.; Panethymitaki, C.; Goulding, D.; McKean, P. G.; Smith, D. F. Myristoyl-CoA:protein *N*-myristoyltransferase, an essential enzyme and potential drug target in kinetoplastid parasites. *J. Biol. Chem.* **2003**, *278*, 7206−7214.

(8) Price, H. P.; Guther, M. L. S.; Ferguson, M. A. J.; Smith, D. F. Myristoyl-CoA:protein *N*-myristoyltransferase depletion in trypanosomes causes avirulence and endocytic defects. *Mol. Biochem. Parasitol.* **2010**, *169*, 55−58.

(9) Bowyer, P. W.; Tate, E. W.; Leatherbarrow, R. J.; Holder, A. A.; Smith, D. F.; Brown, K. A. *N*-Myristoyltransferase: a prospective drug target for protozoan parasites. *ChemMedChem* **2008**, *3*, 402−408.

(10) Price, H. P.; Stark, M.; Smith, D. F. *Trypanosoma brucei* ARF1 plays a central role in endocytosis and golgi-lysosome trafficking. *Mol. Biol. Cell* **2007**, *18*, 864−73.

(11) Wright, M. H.; Clough, B.; Rackham, M. D.; Rangachari, K.; Brannigan, J. A.; Grainger, M.; Moss, D. K.; Bottrill, A. R.; Heal, W. P.; Broncel, M.; Serwa, R. A.; Brady, D.; Mann, D. J.; Leatherbarrow, R. J.; Tewari, R.; Wilkinson, A. J.; Holder, A. A.; Tate, E. W. Validation of *N*-myristoyltransferase as an antimalarial drug target using an integrated chemical biology approach. *Nature Chem.* **2014**, *6*, 112−121.

(12) Tate, E. W.; Bell, A. S.; Rackham, M. D.; Wright, M. H. *N*-Myristoyltransferase as a potential drug target in malaria and leishmaniasis. *Parasitology* **2014**, *141*, 37−49.

(13) Roberts, A. J.; Torrie, L. S.; Wyllie, S.; Fairlamb, A. H. Biochemical and genetic characterisation of *Trypanosoma cruzi N*-myristoyltransferase. *Biochem. J.* **2014**, *459*, 323−332.

(14) Brand, S.; Cleghorn, L. A.; McElroy, S. P.; Robinson, D. A.; Smith, V. C.; Hallyburton, I.; Harrison, J. R.; Norcross, N. R.; Spinks, D.; Bayliss, T.; Norval, S.; Stojanovski, L.; Torrie, L. S.; Frearson, J. A.; Brenk, R.; Fairlamb, A. H.; Ferguson, M. A.; Read, K. D.; Wyatt, P. G.; Gilbert, I. H. Discovery of a novel class of orally active trypanocidal *N*-myristoyltransferase inhibitors. *J. Med. Chem.* **2012**, *55*, 140−152.

(15) Frearson, J. A.; Brand, S.; McElroy, S. P.; Cleghorn, L. A. T.; Smid, O.; Stojanovski, L.; Price, H. P.; Guther, M. L. S.; Torrie, L. S.; Robinson, D. A.; Hallyburton, I.; Mpamhanga, C. P.; Brannigan, J. A.; Wilkinson, A. J.; Hodgkinson, M.; Hui, R.; Qiu, W.; Raimi, O. G.; Van Aalten, D. M. F.; Brenk, R.; Gilbert, I. H.; Read, K. D.; Fairlamb, A. H.; Ferguson, M. A. J.; Smith, D. F.; Wyatt, P. G. *N*-Myristoyltransferase inhibitors as new leads to treat sleeping sickness. *Nature* **2010**, *464*, 728−732.

(16) Polli, J. W.; Jarrett, J. L.; Studenberg, S. D.; Humphreys, J. E.; Dennis, S. W.; Brouwer, K. R.; Woolley, J. L. Role of P-glycoprotein on the CNS disposition of amprenavir (141W94), an HIV protease inhibitor. *Pharm. Res.* **1999**, *16*, 1206−1212.

(17) Di, L.; Rong, H.; Feng, B. Demystifying brain penetration in central nervous system drug discovery. Miniperspective. *J. Med. Chem.* **2013**, *56*, 2−12.

(18) Zakeri-Milani, P.; Tajerzadeh, H.; Islambolchilar, Z.; Barzegar, S.; Valizadeh, H. The relation between molecular properties of drugs and their transport across the intestinal membrane. *DARU J. Pharm. Sci.* **2006**, *14*, 164−171.

(19) Chinchilla, R.; Najera, C. The Sonogashira reaction: a booming methodology in synthetic organic chemistry. *Chem. Rev.* **2007**, *107*, 874−922.

(20) Chemler, S. R.; Trauner, D.; Danishefsky, S. J. The B-Alkyl Suzuki−Miyaura cross-coupling reaction: development, mechanistic study, and applications in natural product synthesis. *Angew. Chem., Int. Ed. Engl.* **2001**, *40*, 4544−4568.

(21) Wang, T.; Bisson, W. H.; Maser, P.; Scapozza, L.; Picard, D. Differences in conformational dynamics between *Plasmodium falciparum* and human Hsp90 orthologues enable the structure-based discovery of pathogen-selective inhibitors. *J. Med. Chem.* **2014**, *57*, 2524−2535.

(22) Brodney, M. A.; Barreiro, G.; Ogilvie, K.; Hajos-Korcsok, E.; Murray, J.; Vajdos, F.; Ambroise, C.; Christoffersen, C.; Fisher, K.; Lanyon, L.; Liu, J.; Nolan, C. E.; Withka, J. M.; Borzilleri, K. A.; Efremov, I.; Oborski, C. E.; Varghese, A.; O'Neill, B. T. Spirocyclic sulfamides as beta-secretase 1 (BACE-1) inhibitors for the treatment of Alzheimer's disease: utilization of structure based drug design,

WaterMap, and CNS penetration studies to identify centrally efficacious inhibitors. *J. Med. Chem.* **2012**, *55*, 9224−9239.
(23) Mattson, M. N.; Neitzel, M. L.; Quincy, D. A.; Semko, C. M.; Garofalo, A. W.; Keim, P. S.; Konradi, A. W.; Pleiss, M. A.; Sham, H. L.; Brigham, E. F.; Goldbach, E. G.; Zhang, H.; Sauer, J. M.; Basi, G. S. Discovery of sulfonamide-pyrazole gamma-secretase inhibitors. *Bioorg. Med. Chem. Lett.* **2010**, *20*, 2148−2150.
(24) Covel, J. A.; Santora, V. J.; Smith, J. M.; Hayashi, R.; Gallardo, C.; Weinhouse, M. I.; Ibarra, J. B.; Schultz, J. A.; Park, D. M.; Estrada, S. A.; Hofilena, B. J.; Pulley, M. D.; Smith, B. M.; Ren, A.; Suarez, M.; Frazer, J.; Edwards, J.; Hauser, E. K.; Lorea, J.; Semple, G.; Grottick, A. J. Design and evaluation of novel biphenyl sulfonamide derivatives with potent histamine H(3) receptor inverse agonist activity. *J. Med. Chem.* **2009**, *52*, 5603−5611.
(25) Peters, R.; Wakelin, R. W. Biochemistry of fluoroacetate poisoning; the isolation and some properties of the fluorotricarboxylic acid inhibitor of citrate metabolism. *Proc. R. Soc. London B, Biol. Sci.* **1953**, *140*, 497−507.
(26) Read, K. D.; Braggio, S. Assessing brain free fraction in early drug discovery. *Expert. Opin. Drug. Metab. Toxicol.* **2010**, *6*, 337−344.
(27) Hughes, J. D.; Blagg, J.; Price, D. A.; Bailey, S.; Decrescenzo, G. A.; Devraj, R. V.; Ellsworth, E.; Fobian, Y. M.; Gibbs, M. E.; Gilles, R. W.; Greene, N.; Huang, E.; Krieger-Burke, T.; Loesel, J.; Wager, T.; Whiteley, L.; Zhang, Y. Physiochemical drug properties associated with in vivo toxicological outcomes. *Bioorg. Med. Chem. Lett.* **2008**, *18*, 4872−4875.
(28) Panethymitaki, C.; Bowyer, P. W.; Price, H. P.; Leatherbarrow, R. J.; Brown, K. A.; Smith, D. F. Characterization and selective inhibition of myristoyl-CoA: protein *N*-myristoyltransferase from *Trypanosoma brucei* and *Leishmania major*. *Biochem. J.* **2006**, *396*, 277−285.
(29) Raz, B.; Iten, M.; Grether-Buhler, Y.; Kaminski, R.; Brun, R. The Alamar Blue assay to determine drug sensitivity of African trypanosomes (*T. b. rhodesiense* and *T. b. gambiense*) in vitro. *Acta Trop.* **1997**, *68*, 139−147.
(30) Hirumi, H.; Hirumi, K. Continuous cultivation of *Trypanosoma brucei* blood stream forms in a medium containing a low concentration of serum-protein without feeder cell-layers. *J. Parasitol.* **1989**, *75*, 985−989.
(31) Jennings, F. W.; Chauviere, G.; Viode, C.; Murray, M. Topical chemotherapy for experimental African trypanosomiasis with cerebral involvement: the use of melarsoprol combined with the 5-nitro-imidazole, megazol. *Trop. Med. Int. Health* **1996**, *1*, 363−366.
(32) Sanderson, L.; Dogruel, M.; Rodgers, J.; Bradley, B.; Thomas, S. A. The blood−brain barrier significantly limits eflornithine entry into *Trypanosoma brucei brucei* infected mouse brain. *J. Neurochem.* **2008**, *107*, 1136−1146.
(33) Jennings, F. W.; Gray, G. D. Relapsed parasitaemia following chemotherapy of chronic *T. brucei* infections in mice and its relation to cerebral trypanosomes. *Contrib. Microbiol. Immunol.* **1983**, *7*, 147−154.
(34) Gichuki, C.; Brun, R. Animal models of CNS (second-stage) sleeping sickness. In *Handbook of Animal Models of Infection*; Zak, O., Sande, M., Eds.; Academic Press: London, 1999; pp 795−800.